



Fe₃O₄/functional exfoliation graphene on carbon paper nanocomposites for supercapacitor electrode

Yanfei Li¹ · Jie Yu¹ · Shouhui Chen¹ · Zhenzhong Huang¹ · Li Wang¹

Received: 30 October 2017 / Revised: 10 December 2017 / Accepted: 13 December 2017 / Published online: 23 December 2017
© Springer-Verlag GmbH Germany, part of Springer Nature 2017

Abstract

In this work, the commercial carbon paper was firstly peeled in K₂CO₃ solution and then was further treated in a KNO₃ solution to form functional exfoliation graphene (FEG) on the commercial carbon paper. The FEG/carbon paper was characterized by Raman spectra and scanning electron microscopy, confirming that some typical layered fold graphenes were successfully peeled off and stood on the carbon paper matrix. Then, Fe₃O₄ nanoparticles (NPs) were grown on the surface of FEG/carbon paper and the as-prepared Fe₃O₄ NPs/FEG/carbon paper was directly used as supercapacitor electrode. The specific capacitance of Fe₃O₄ NPs/FEG/carbon paper was about 316.07 F g⁻¹ at a current density of 1 A g⁻¹. Furthermore, the FEG/carbon papers were also functionalized by benzene carboxylic acid to form FFEG/carbon papers, and then the Fe₃O₄ NPs were grown on the surface of FFEG/carbon paper. The specific capacitance of Fe₃O₄ NPs/FFEG/carbon paper was 470 F g⁻¹ at a current density of 1 A g⁻¹, superior to some previous reported results. This work might provide a new strategy to prepare various nanostructures on FFEG/carbon papers for future applications.

Keywords Graphene · Electrochemistry · Carbon paper · Supercapacitor · Fe₃O₄ nanoparticles

Introduction

In recent years, researchers have been exploring various novel energy storage materials to meet the needs of renewable energy resources, and portable electronic devices [1, 2]. Supercapacitor, a kind of promising energy storage device, has been receiving more and more attention due to its high-power density, rapid charging and discharging rate, long cycle life, and wide working temperature range [3–10].

Supercapacitors are usually divided into double-layer capacitors and pseudocapacitors [11]. The double-layer capacitor materials are mainly carbon materials such as graphite,

graphene, reduced graphene oxide (rGO), carbon nanotubes (CNTs), carbon nanofibers (CNFs), and porous carbon [5, 12–14]. Among various carbon materials, graphene or rGO with good electrical conductivity, large specific surface area (about 2630 m² g⁻¹), high flexibility as well as chemical and thermal stability has been applied widely for supercapacitors [15–19]. For example, the cross-linked N-doped graphene showed superior capacitive performance [20]. Various preparation methods have been developed to prepare graphene and rGO, such as chemical vapor deposition [21–23], epitaxial growth method [24–27], chemical/thermal reduction method [28, 29], and solvent hot method [30, 31]. However, these methods are very complicated and the specific capacitance of the as-obtained graphene and rGO is low. And its stability and mechanical properties of graphene are relatively poor owing to the weak interaction between the graphenes, which increases contact resistance between nanosheets and substrates. As a result, the cycle performance and the energy density of capacitor are very poor.

Pseudocapacitor electrode materials mainly come from redox-active materials, including conducting polymers [32, 33] and metal oxide nanoparticles (NPs) (Fe₃O₄ NPs, Co₃O₄ NPs, etc.) [34–38]. Among various metal oxides, Fe₃O₄ is an important one for supercapacitors because of its low cost,

Electronic supplementary material The online version of this article (<https://doi.org/10.1007/s11581-017-2409-y>) contains supplementary material, which is available to authorized users.

✉ Li Wang
lwanggroup@aliyun.com

¹ Key Laboratory of Functional Small Organic Molecule, Ministry of Education, Key Laboratory of Chemical Biology, Jiangxi Province, College of Chemistry and Chemical Engineering, Jiangxi Normal University, Nanchang 330022, China

abundance, environmental compatibility, and high theoretical capacity. Accordingly, various Fe₃O₄ NPs have been extensively investigated as the electrode materials for a supercapacitor. For example, Wang et al. prepared Fe₃O₄ NPs by using FeCl₃ and ethanolamine and it exhibited remarkable pseudocapacitive activities [39]. However, Fe₃O₄ NPs just provide a low capacitance (< 300 F g⁻¹) in aqueous electrolyte due to their poor electrical conductivity. As we all know, incorporating Fe₃O₄ NPs into carbon materials with good electrical conductivity could improve their capacitance performance significantly [34, 35]. For example, Fe₃O₄-doped graphene showed desired capacitance and high-energy density [35]. The hybrid of Fe₃O₄-doped porous carbon nanorods supported by three-dimensional (3D) kenaf stem-derived macroporous carbon exhibited 220.5 F g⁻¹ after 5000 cycles at 2.0 A g⁻¹ [40]. MIL-88A-derived Fe₃O₄-carbon hierarchical nanocomposites were also applied for electrochemical sensing, and it also showed good performance [41]. Thus, the design of novel Fe₃O₄/carbon nanocomposite is very significant for achieving high performance of supercapacitors.

In this work, the commercial carbon paper which was composed of graphene layers was treated by a two-step electrochemical peeled method to form functional exfoliation graphene (FEG). Some typical layered fold graphenes were successfully peeled off and stood on the carbon paper matrix to form 3D graphene foam. The peeled graphene provided a large surface area and greatly improved the electron transfer ability of pseudocapacitance materials. Then, the FEG/carbon papers were further functionalized by benzene carboxylic acid to form FFEG/carbon papers. Finally, a large number of small Fe₃O₄ NPs were grown on the surface of FFEG/carbon paper. The as-synthesized Fe₃O₄ NPs/ FFEG/carbon paper nanocomposites were directly used as supercapacitor electrode. The specific capacitance was about 470 F/g⁻¹ under current density of 1 A g⁻¹, and it still maintained 432 F g⁻¹ after 5000 cycles.

Experimental

Reagents and materials

Commercial carbon papers were obtained from Physical and Chemical Company (Hong Kong, China). FeCl₃·6H₂O, KNO₃, K₂CO₃, and p-aminobenzoic acid were purchased from Aladdin Chemistry Co., (Ltd Shanghai, China). NaAc, ethylene glycol, Na₂SO₄, Na₂HPO₃, and NaH₂PO₃ were purchased from Sinopharm Chemical Reagent (Shanghai, China). Other reagents of analytical grade were obtained from Shanghai Reagent Co., Ltd. (Shanghai, China). All reagents were of analytical grade and used as received. Platinum sheet electrode holder was obtained from Tianjin Joint Company

(Tianjin, China). All solutions were prepared with ultrapure water, purified by a Millipore-Q system (18.2 MΩ cm).

Characterization

Scanning electron microscopy (SEM) images were obtained with a Hitachi S3400N at an accelerating voltage of 20 kV equipped with an energy dispersive spectrometer (EDS). Raman spectra were recorded on a LabRAM HR (Horiba Jobin Yvon) with a 633-nm laser. Cyclic voltammograms (CVs), electrochemical impedance spectroscopy (EIS), and constant current charging/discharging tests (CP) were performed using a CHI760e electrochemical workstation (CH Instruments Inc., China) at room temperature. CVs and CP were carried out in 1 M Na₂SO₃ with a three-electrode system by using Fe₃O₄ NPs/FFEG/carbon paper as the working electrode, a saturated calomel electrode (SCE) as the reference electrode, and a platinum electrode as the counter electrode. And the binder was not used in the electrode preparation. EIS measurements were performed in 0.1 M KCl containing 5.0 mM Fe(CN)₆^{3-/4-} in the frequency range from 100 kHz to 0.1 Hz at open circuit potential by applying a 5-mV signal. CP tests were tested at different current density at the potential window between -0.6 V and 0.1 V. The specific capacitance of single electrode was calculated according to the following Eq. (1) (galvanostatic charge/discharge curves):

$$C_s = \frac{I\Delta t}{m(V_a - V_c)} \quad (1)$$

where C_s is the specific capacitance (F g⁻¹), m is the mass of Fe₃O₄ (g), $(V_a - V_c)$ represents the potential window (V), I is the discharge current (A), and Δt is the discharge time (s).

Preparation of FEG/carbon paper

Firstly, the commercial carbon papers were pre-treated by ultrasound in acetone, ethanol, and distilled water, respectively, and then dried at 60 °C. After that, the carbon paper was cut into small pieces with 1 × 1.5 cm size. The two-step peeled method was carried out by using carbon paper as the working electrode whose working area was 1 × 1 cm² (Fig. S1, Supporting Information). The carbon paper electrode was firstly treated by CVs scan in 0.5 M K₂CO₃ solution at the scanning potential from 0.5 to 1.8 V at the scan rate of 20 mV s⁻¹ for 6 cycles. Next, it was further scanned in 1.0 M KNO₃ solution at the scanning potential of -0.9–1.9 V at the scan rate of 20 mV s⁻¹ for 20 cycles. Finally, the carbon paper was removed out and rising by ultrapure water to remove off inorganic residues. The carbon paper electrode was dried in the oven to obtain the FEG/carbon paper for next time. The preparation process of FEG/carbon paper was illustrated in Fig. 1.

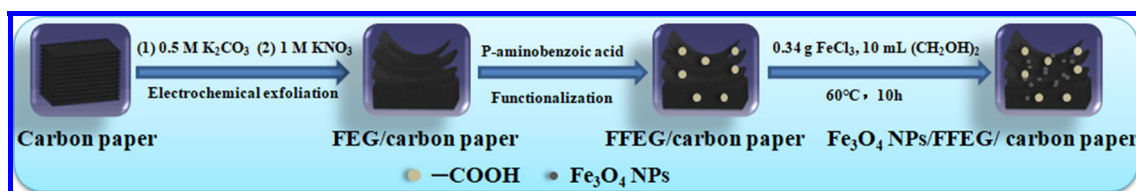


Fig. 1 Schematic illustration of fabrication process of Fe_3O_4 NPs/FFEG/carbon paper

Benzene carboxylic acid functionalized FEG/carbon paper

The 4-benzoate diazonium salt was prepared as follows. The p-aminobenzoic acid (480 mg) was firstly dissolved in 40 mL ultrapure water solution which contained NaOH (140 mg). Then, 236 mg NaNO_2 was slowly added into the above solution in the condition of ice bath. After that, 6.4 M HCl (3 mL) was quickly added. After 45 min, the light yellow 4-benzoate diazonium salt was obtained. The FEG/carbon paper electrode was immersed in the above 4-benzoate diazonium salt and scanned at the working potential window between -0.60 and 0.3 V for scanning 20 cycles at the scan rate of 100 mV s^{-1} . After 20 cycles, the 4-benzene acid was grafted to FEG/carbon paper by electrochemical reduction and growth to form the FFEG/carbon paper. The preparation process of FFEG/carbon paper was illustrated in Fig. 1.

Preparation of Fe_3O_4 NPs/FFEG/carbon paper

The growth of Fe_3O_4 NPs on FFEG/carbon paper was carried out as follows. Firstly, 0.34 g FeCl_3 was mixed with 10 mL ethylene glycol under stirring for 10 min. The solution was

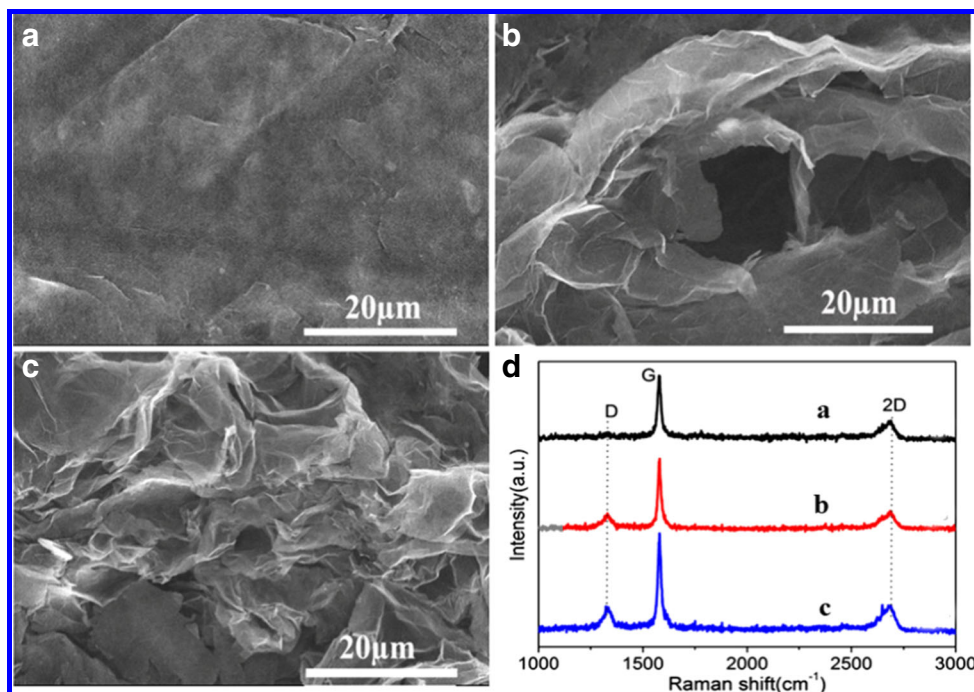
then added into 0.25 g NaAc under ultrasound. After that, the hybrid solution was transformed into 25 mL Teflon-lined stainless steel and then the as-prepared FFEG/carbon paper (250 mg) was immersed in the Teflon-lined stainless to make the solution cover FFEG/carbon paper absolutely. Subsequently, the Teflon-lined stainless steel was put in the oven and reacted at 200°C . After 10 h, the FFEG/carbon paper was taken out and rinsed by ethanol and water several times to obtain the Fe_3O_4 NPs/FFEG/carbon paper. The weight of Fe_3O_4 NPs loaded on the FFEG/carbon paper was obtained according to the quality of FFEG/carbon paper before and after loading. As a comparison, the Fe_3O_4 NPs/FEG/carbon paper was also prepared by the same procedure. The preparation process of Fe_3O_4 NPs/FFEG/carbon paper was illustrated in Fig. 1.

Results and discussion

The characterization of FFEG/carbon paper

The preparation of FEG/carbon paper was monitored by CVs. As shown in Fig. S2A (Supporting Information), the current

Fig. 2 SEM images of carbon paper (a), FEG/carbon paper prepared by the first step (b), and FEG/carbon paper prepared by two steps (c). Raman spectra of carbon paper (curve a) (d), FEG/carbon paper prepared by the first step (curve b), and FEG/carbon paper prepared by two steps (curve c)



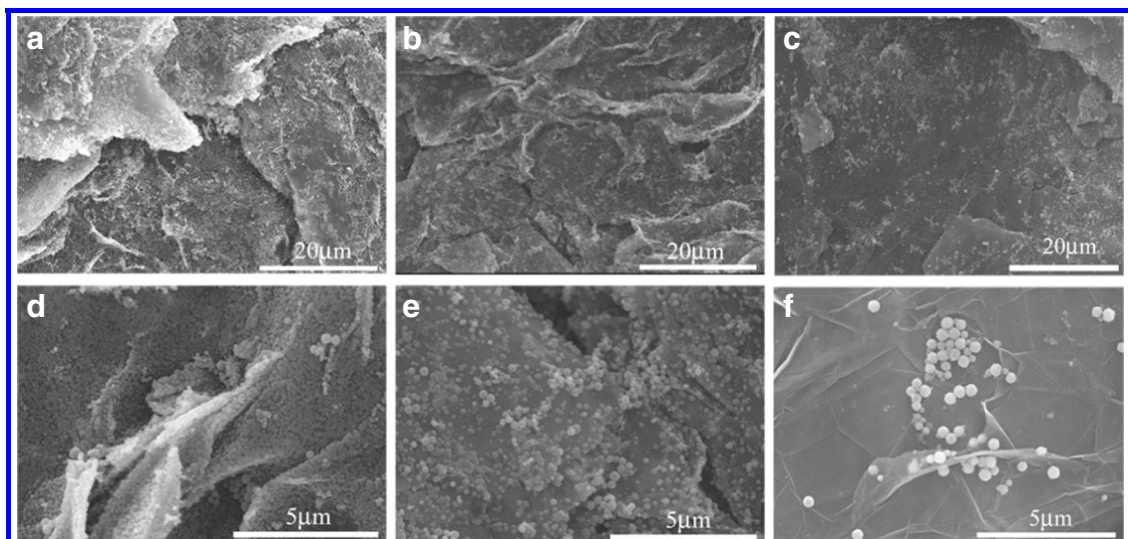


Fig. 3 SEM images of (a, d) Fe_3O_4 NPs/FFEG/carbon paper, (b, e) Fe_3O_4 NPs/FEG/carbon paper, and (c, f) Fe_3O_4 NPs/carbon paper

started to increase at about 1.1 V and rapidly raised near 1.2 V, which was attributed to the oxygen evolution reaction. Therefore, it produced lots of oxygen around the carbon paper surface. Due to many defects around the periphery of carbon paper, the small bubbles of oxygen made graphene partly to be peeled off. Finally, 3D graphene foam was formed on carbon paper after six CVs. Then, the electrode was transferred in 1.0 M KNO_3 and was cycled in the scanning potential of -0.9 – 1.9 V at the scanning rate of 20 mV^{-1} . As shown in Fig. S2B (Supporting Information), the current rapidly raised near 1.2 V, indicating the graphene continued to be peeled off. In the reverse scan, several peaks were found and they could be ascribed to the reduction of oxygen-containing groups on carbon paper. Figure S3 (Supporting Information) showed the CVs of obtained FEG/carbon paper electrode in 4-benzoate diazonium salt solution scanned in the working potential window between -0.60 and 0.3 V for 20 cycles. As shown in Fig. S3 (Supporting Information), a reduction peak was found at -0.1 V which was attributed to the reduction of 4-benzene

carboxylic diazonium salt cations. In the reverse scan, an oxidation peak appeared at 0.2 V which was attributed to the oxidation of benzene carboxylic. With the increase of scanning cycles, cathodic peak current decreased and the cathode potential was gradually moving in the positive direction, indicating 4-benzene carboxylic functional group was successfully modified on the surface of FEG to form FFEG/carbon paper.

As shown in Fig. 2a, the surface of carbon paper was very smooth and no typical graphene layer was observed. After the first step to peel off, some typical graphene layers were peeled off by the production of oxygen bubble (Fig. 2b). The large hole might originate from the oxygen bubble. The parts of graphene layers still stood on the surface of carbon paper. After the secondary oxidation stripping, more graphene layers were produced and they formed 3D graphene foam (Fig. 2c). Such 3D porous structure could promote diffusion of ions and accordingly it was helpful to the transfer of electrochemical active materials and provided a large specific surface area.

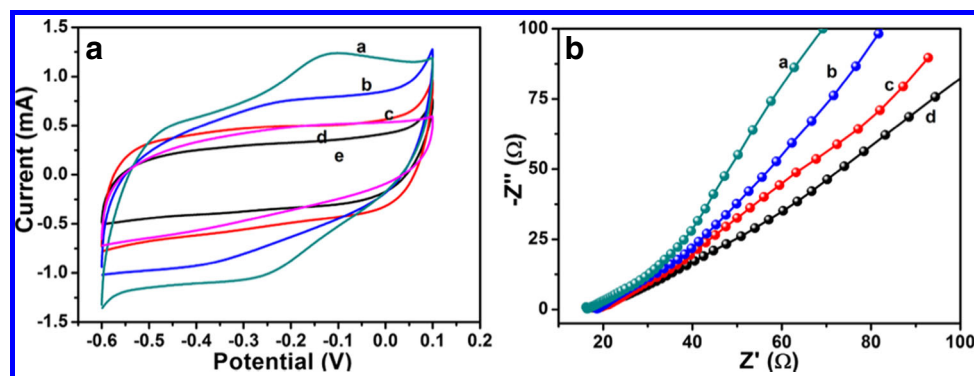


Fig. 4 a CVs of Fe_3O_4 NPs/FFEG/carbon paper (curve a), Fe_3O_4 NPs/FEG/carbon paper (curve b), FFEG/carbon paper (curve c), Fe_3O_4 NPs/carbon paper (curve d), and carbon paper (curve e) in 1 M Na_2SO_3 at the scanning rate of 10 mV s^{-1} . b The Nyquist plots of

Fe_3O_4 NPs/FFEG/carbon paper (curve a), Fe_3O_4 NPs/FEG/carbon paper (curve b), FEG/carbon paper (curve c), and carbon paper (curve d) in $5.0 \text{ mM Fe(CN)}_6^{3-/4-}$ at the scanning frequency range from 0.01 Hz to 10.0 KHz

Figure 2d showed the Raman spectra of three materials. Three peaks belonged to carbon materials was found and they corresponded to D band, G band and 2D band, respectively [42]. The D band was attributed to the rotation of plane carbon atom, which showed the edge flaw of graphene. The higher intensity of D peak came from the greater disordering degree of the material. It was obvious that the intensity of D band was enhanced after two-step stripping, indicating more and more defect structures and the successful formation of graphene.

Figure 3 showed SEM images of Fe₃O₄ NPs/FFEG/carbon paper, Fe₃O₄ NPs/FEG/carbon paper, and Fe₃O₄ NPs/carbon paper. As shown in Fig. 3a, d, a large number of small Fe₃O₄ NPs was formed and uniformly dispersed on FFEG/carbon paper. XRD pattern of Fe₃O₄ NPs/FEG/carbon paper showed diffraction peaks at 30.1°, 35.4°, 43.1°, 56.9°, 62.5°, and 74.9° (Fig. S4, Supporting Information). The diffraction peaks were ascribed to the (220), (311), (400), (511), (440), and (533) crystalline facets of Fe₃O₄ (JCPDS No. 19-0629) [43], and the (002), (004) crystalline facets of FFEG/carbon paper. The result proved that Fe₃O₄ NPs were synthesized successfully on the FFEG/carbon paper. While, there also were lots of Fe₃O₄ NPs uniformly dispersed on the surface of FEG/carbon paper (Fig. 3b, e). As compared with that on FFEG/carbon paper, the amounts of Fe₃O₄ NPs on FEG/carbon paper were fewer and the size of Fe₃O₄ NPs was larger. The result confirmed that the –COOH groups of FFEG/carbon paper was benefit for the growth and distribution of Fe₃O₄ NPs. However, only a few large Fe₃O₄ NPs formed on carbon paper and they were prone to aggregated (Fig. 3c, f). The result indicated that many flaw sites were also formed on graphene when they were peeled off. The defect sites might be used as

Fig. 5 Constant current charge/discharge curves of **a** Fe₃O₄ NPs/FFEG/carbon paper, **b** Fe₃O₄ NPs/FEG/carbon paper, and **c** Fe₃O₄ NPs/carbon paper materials in 1 M Na₂SO₃ solution at a current density of 1.0, 1.25, 2.5, 5.0, and 6.25 A g⁻¹. **d** The plots of specific capacitance of various materials versus different current densities

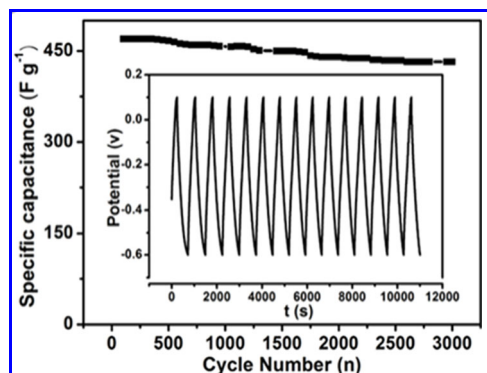
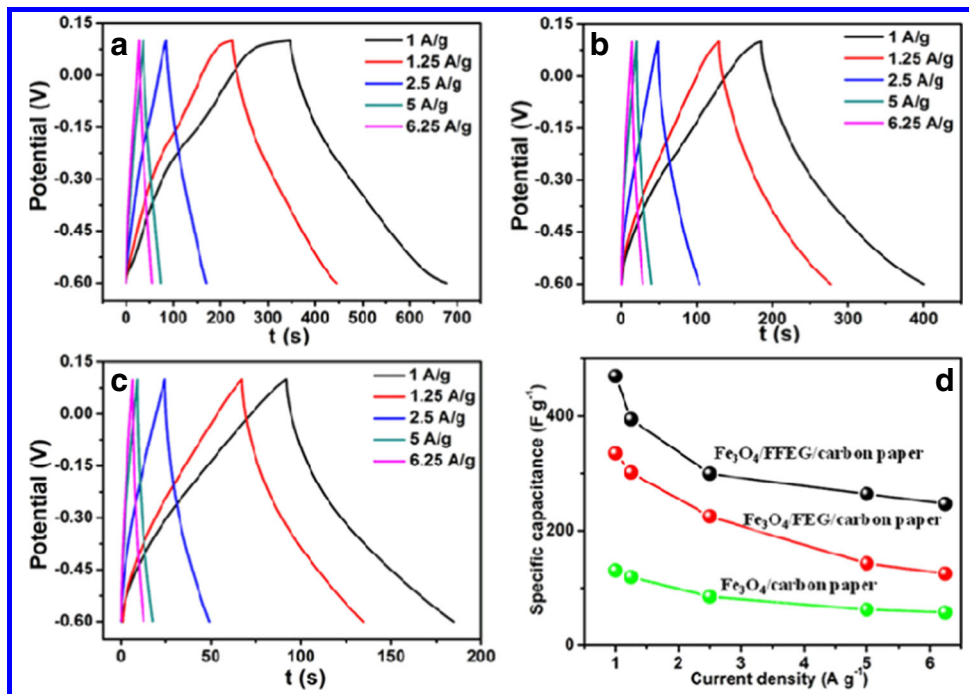


Fig. 6 Cycle performance of Fe₃O₄ NPs/FFEG/carbon paper at a current density of 1.0 A g⁻¹. The electrolyte was 1.0 M Na₂SO₃

anchored sites to guide the growth and distribution of small Fe₃O₄ NPs. Accordingly, many relatively small Fe₃O₄ NPs were also formed on Fe₃O₄ NPs/FEG/carbon paper.

Electrochemical behaviors of Fe₃O₄ NPs/FFEG/carbon paper

CV and EIS were firstly used to explore electrochemical performance of Fe₃O₄ NPs/FFEG/carbon paper as supercapacitor electrode. As shown in Fig. 4a, a pair of obvious redox peaks was found at Fe₃O₄ NPs/FFEG carbon paper (curve a) and they might be ascribed to the redox of Fe₃O₄ NPs since no peak was observed on FFEG/carbon paper (curve c) and carbon paper (curve e). Although the pair of redox peaks was also observed on Fe₃O₄ NPs/FEG/carbon paper (curve b), it was smaller than that of Fe₃O₄ NPs/FFEG/carbon paper. It was very difficult to observe the pair redox peaks on the Fe₃O₄

Table 1 Comparison of the performance of various based-Fe₃O₄ NPs supercapacitors

Materials	Capacitance (F/g)	Current density (A/g)	Cycle life (F/g)	Reference
Fe ₃ O ₄ @few layer graphene/PEDOT:PSS	153	0.1	174.42 after 3500 cycles at 1 A g ⁻¹	[44]
Hexagon-Fe ₃ O ₄ sheets/rGO	193	0.3	174.5 after 1000 cycles at 5 A g ⁻¹	[45]
Co ₂ AlO ₄ @MnO ₂ nanosheets and Fe ₃ O ₄ nanoflakes/nickel foam	99.1	2	91.5 after 5000 cycles at 1 A g ⁻¹	[46]
Hollow Fe ₃ O ₄ sub-micron spheres	294	0.5	266.9 after 500 cycles at 0.4 A g ⁻¹	[47]
Fe ₃ O ₄ /carbon nanorods	275.9	0.5	30 after 500 cycles at 0.5 A g ⁻¹	[48]
Fe ₃ O ₄ /CNFs nanocomposites	135	0.42	120 after 1000 cycles at 0.4 A g ⁻¹	[49]
Fe ₃ O ₄ /rGO nanocomposites	480	5.0	538 after 1000 cycles at 5 A g ⁻¹	[50]
Fe ₃ O ₄ /rGO multilayer film	250	0.5	212 after 1000 cycles at 0.5 A g ⁻¹	[51]
Fe ₃ O ₄ NPs/FFEG carbon paper	470	1	432 after 5000 cycles at 1 A g ⁻¹	This work

NPs/carbon paper because only a few large Fe₃O₄ NPs on carbon paper (curve d). The results clearly indicated that all the materials have the large capacitance but the capacitance of Fe₃O₄ NPs/FFEG/carbon paper was biggest. Figure 4b showed Nyquist plots of various materials. All the materials showed small impedance because no semi-circle was found on these curves but the ion diffusion rate of Fe₃O₄ NPs/FFEG/carbon paper was the biggest. The rapid ion diffusion rate was a benefit for the performance of supercapacitors.

Figure 5 showed that the constant current charge/discharge curves of Fe₃O₄ NPs/FFEG carbon paper (Fig. 5a), Fe₃O₄ NPs/FEG/carbon paper (Fig. 5b), and Fe₃O₄ NPs/carbon paper (Fig. 5c) electrodes in the potential range of -0.6–0.1 V at various specific current densities. All the materials gave the significant constraint capacitance platform. The specific capacitance of Fe₃O₄ NPs/FFEG carbon paper was 470, 394.64, 299.64, 264.29, and 246.43 F g⁻¹ at the current density of 1, 1.25, 2.5, 5, and 6.25 A g⁻¹, respectively (Fig. 5a). The capacitance of Fe₃O₄ NPs/FEG/carbon paper under the different current densities was 335, 301.79, 225, 142.85, 125 F g⁻¹ (Fig. 5b) and the capacitance of Fe₃O₄ NPs/carbon paper in various current densities was 130.71, 119.29, 85.35, 62.28, and 57.32 F g⁻¹ (Fig. 5c). As shown in Fig. 5d and Fig. S5 (Supporting Information), the Fe₃O₄ NPs/FFEG/carbon paper showed the largest capacitance, which could be ascribed to the 3D porous structures and loading largest amount of small Fe₃O₄ NPs. Figure S6 (Supporting Information) showed that the reaction time of 10 h was optimal.

Next, the cycle life of Fe₃O₄ NPs/FFEG/carbon paper was tested (Fig. 6). The constant current charge/discharge test was carried out under the current density of 1 A g⁻¹ for 5000 cycles. The capacitance slightly decreased to 432 F g⁻¹. The good stability might be ascribed to the firm immobilization of Fe₃O₄ NPs on -COOH groups of FFEG, the firm graphene foam on carbon paper as well as uniform distribution of small Fe₃O₄ NPs. Figure S7 displayed CVs of Fe₃O₄ NPs/FFEG/carbon paper at various scan rates. With the increasing scan rates, the anodic peaks shift toward positive potential and the cathodic peaks shift toward negative potential due to the electrode polarization at larger scan rates. The current linearly increased as the scan rate increased, indicating a good rate capability. To exhibit the advantage of proposed materials, the performance of different FeOx nanocomposites based supercapacitors were compared in Table 1. By comparing, the Fe₃O₄ NPs/FFEG carbon paper showed the largest specific capacitance because both 3D porous structure and small and uniformly distributed Fe₃O₄ NPs promoted the electron and mass transfer together. What's more, the 3D graphene foam and -COOH groups of FFEG also provided a larger surface area to load a large number of small Fe₃O₄ NPs effectively, which improved the utilization efficiency of the active

material largely and avoided the aggregation of Fe₃O₄ NPs in the charge/discharge process.

Conclusion

In summary, a simple two-step electrochemical peeled method to form FFEG/carbon paper was developed to load Fe₃O₄ NPs as supercapacitor electrode. Some typical layered fold graphenes were successfully peeled off and stood on the carbon paper matrix to form 3D graphene foam. The Fe₃O₄ NPs/FFEG/carbon paper as a free-binder electrode for supercapacitors exhibited the following advantages. Firstly, both the porous structure and the good conductivity of 3D graphene foam were a benefit for electron and mass transfer. Secondly, the 3D graphene foam could effectively alleviate the agglomeration of Fe₃O₄ NPs and accordingly improve the performance of the supercapacitors. Thirdly, the 3D graphene foam and a large number of –COOH groups of FFEG provided a larger surface area to load a large number of small Fe₃O₄ NPs effectively, which improved the utilization efficiency of the active material largely. Fourthly, the firm immobilization of Fe₃O₄ NPs on –COOH groups of FFEG, the firm graphene foam on carbon paper as well as uniform distribution of small Fe₃O₄ NPs resulted in good stability. Finally, the 3D graphene foam served not only as the supporting of Fe₃O₄ NPs but also as the current collector of the supercapacitors, which would reduce the costs. As a result, the Fe₃O₄ NPs/FFEG/carbon paper exhibited a high-specific capacitance of 470 F g^{−1} at the current density of 1 A g^{−1}, which was much higher than other carbon materials. Moreover, the good cycle performance indicated that the newly developed supercapacitors based on the Fe₃O₄ NPs/FFEG/carbon paper might be potentially useful for future energy storage applications.

Funding information This work was financially supported by the National Natural Science Foundation of China (21465014, and 21765009), the Natural Science Foundation of Jiangxi Province (20143ACB21016), and the Ground Plan of Science and Technology Projects of Jiangxi Educational Committee (KJLD14023).

References

- CJ H, Song L, Zhang ZP, Chen N, Feng ZH, LT Q (2015) Tailored graphene systems for unconventional applications in energy conversion and storage devices. *Energy Environ Sci* 8:31–54
- Liu M, Ma XM, Gan LH, ZJ X, Zhu DZ, Chen LW (2014) A facile synthesis of a novel mesoporous Ge@C sphere anode with stable and high capacity for lithium ion batteries. *J Mater Chem A* 2(40): 17107–17114. <https://doi.org/10.1039/C4TA02888K>
- Liu CG, ZN Y, Neff D, Zhamu A, Jang BZ (2010) Graphene-based supercapacitor with an ultrahigh energy density. *Nano Lett* 10(12): 4863–4868. <https://doi.org/10.1021/nl102661q>
- Wang Y, Shi ZQ, Huang Y, Ma YF, Wang CY, Chen MM, Chen YS (2009) Supercapacitor devices based on graphene materials. *J Phys Chem C* 113(30):13103–13107. <https://doi.org/10.1021/jp902214f>
- Zhang LL, Zhao XS (2009) Carbon-based materials as supercapacitor electrodes. *Chem Soc Rev* 38(9):2520–2531. <https://doi.org/10.1039/b813846j>
- Tang C, Pu ZH, Liu Q, Asiri AM, Sun XP, Luo YL, He YQ (2015) In situ growth of NiSe nanowire film on nickel foam as an electrode for high-performance supercapacitors. *ChemElectroChem* 2(12): 1903–1907. <https://doi.org/10.1002/celec.201500285>
- Hou JH, Cao CB, Idrees F, Ma XL (2015) Hierarchical porous nitrogen-doped carbon nanosheets derived from silk for ultrahigh-capacity battery anodes and supercapacitors. *ACS Nano* 9(3):2556–2564. <https://doi.org/10.1021/nn506394r>
- Liu D, Zeng C, DY Q, Tang HL, Li Y, BL S, DY Q (2016) Highly efficient synthesis of ordered nitrogen-doped mesoporous carbons with tunable properties and its application in high performance supercapacitors. *J Power Sources* 321:143–154. <https://doi.org/10.1016/j.jpowsour.2016.04.129>
- Zhao YH, Liu MX, Deng XX, Miao L, Tripathi PK, Ma XM, Zhu DZ, ZJ X, Hao ZX, Gan LH (2015) Nitrogen-functionalized microporous carbon nanoparticles for high performance supercapacitor electrode. *Electrochim Acta* 153:448–455. <https://doi.org/10.1016/j.electacta.2014.11.173>
- Liu S, Guo SJ, Sun SH, You XZ (2015) Dumbbell-like Au-Fe₃O₄ nanoparticles: a new nanostructure for supercapacitors. *Nano* 7: 4890–4893
- Frackowiak E (2007) Carbon materials for supercapacitor application. *Phys Chem Chem Phys* 9(15):1774–1785. <https://doi.org/10.1039/b618139m>
- Huang Y, Liang J, Chen Y (2012) An overview of the applications of graphene-based materials in supercapacitors. *Small* 8(12):1805–1834. <https://doi.org/10.1002/sml.201102635>
- Dai L, Chang DW, Baek JB, Lu W (2012) Carbon nanomaterials for advanced energy conversion and storage. *Small* 8(8):1130–1166. <https://doi.org/10.1002/sml.201101594>
- Jiang H, Lee PS, Li C (2012) 3D carbon based nanostructures for advanced supercapacitors. *Energy Environ Sci* 6:41–53
- Zhang Z, Xiao F, Guo Y, Wang S, Liu Y (2013) One-pot self-assembled three-dimensional TiO₂-graphene hydrogel with improved adsorption capacities and photocatalytic and electrochemical activities. *ACS Appl Mater Inter* 5(6):2227–2233. <https://doi.org/10.1021/am303299r>
- Zhang Z, Xiao F, Qian L, Xiao J, Wang S, Liu Y (2014) Facile synthesis of 3D MnO₂-graphene and carbon nanotube-graphene composite networks for high-performance, flexible, all-solid-state asymmetric supercapacitors. *Adv Energy Mater* 4:1400064
- Zhang Z, Xiao F, Wang S (2015) Hierarchically structured MnO₂/graphene/carbon fiber and porous graphene hydrogel wrapped copper wire for fiber-based flexible all-solid-state asymmetric supercapacitors. *J Mater Chem A* 3(21):11215–11223. <https://doi.org/10.1039/C5TA02331A>
- Zhang Z, Xiao F, Xiao J, Wang S (2015) Functionalized carbonaceous fibers for high performance flexible all-solid-state asymmetric supercapacitors. *J Mater Chem A* 3(22):11817–11823. <https://doi.org/10.1039/C5TA01990G>
- Zhang Z, Chi K, Xiao F, Wang S (2015) Advanced solid-state asymmetric supercapacitors based on 3D graphene/MnO₂ and graphene/polypyrrole hybrid architectures. *J Mater Chem A* 3(24):12828–12835. <https://doi.org/10.1039/C5TA02685G>
- Sun Y, Xing Z, Jiang S, Zhang H, Wei G, Li Z, Zhang X (2016) Rapid preparation of crosslinked N-doped graphene by burning method for high-performance electrochemical capacitors. *Electrochim Acta* 192:243–250. <https://doi.org/10.1016/j.electacta.2016.01.198>

21. Purwidyantri A, Chen CH, Hwang BJ, Luo JD, Chiou CC, Tian YC, Lai CS (2016) Spin-coated Au-nanohole arrays engineered by nanosphere lithography for a *Staphylococcus aureus* 16S rRNA electrochemical sensor. *Biosens Bioelectron* 77:1086–1094. <https://doi.org/10.1016/j.bios.2015.10.094>
22. Liu YL, Jin ZH, Liu YH, XB H, Qin Y, JQ X, Huang WH (2016) Stretchable electrochemical sensor for real-time monitoring of cells and tissues. *Angew Chem* 128(14):4613–4617. <https://doi.org/10.1002/ange.201601276>
23. Jiang GP, Goledzinowski M, Comeau FJE, Zarrin H, Lui G, Lenos J, Qiao J (2016) Free-standing functionalized graphene oxide solid electrolytes in electrochemical gas sensors. *Adv Funct Mater* 26(11):1729–1736. <https://doi.org/10.1002/adfm.201504604>
24. Nguyen TT, Deivasigamani RK, Kharismadewi D, Iwai Y, Shim JJ (2016) Facile synthesis of cobalt oxide/reduced graphene oxide composites for electrochemical capacitor and sensor applications. *Solid State Sci* 53:71–77. <https://doi.org/10.1016/j.solidstatesciences.2016.01.006>
25. Wang Y, Zhang S, Bai W, Zheng J (2016) Layer-by-layer assembly of copper nanoparticles and manganese dioxide-multiwalled carbon nanotubes film: a new nonenzymatic electrochemical sensor for glucose. *Talanta* 149:211–216. <https://doi.org/10.1016/j.talanta.2015.11.040>
26. Zaidi SA, Shin JH (2016) Recent developments in nanostructure based electrochemical glucose sensors. *Talanta* 149:30–42. <https://doi.org/10.1016/j.talanta.2015.11.033>
27. Sun JY, Liu Y, Lv S, Huang Z, Cui L, Wu T (2016) An electrochemical sensor based on nitrogen-doped carbon nanofiber for bisphenol A determination. *Electroanalysis* 28(3):439–444. <https://doi.org/10.1002/elan.201500287>
28. Bakker E, Telting-Diaz M (2002) Electrochemical sensors. *Anal Chem* 74(12):2781–2800. <https://doi.org/10.1021/ac0202278>
29. Reisberg S, Piro B, Noel V, Noël V, Pham MC (2005) DNA electrochemical sensor based on conducting polymer: dependence of the “signal-on” detection on the probe sequence localization. *Anal Chem* 77(10):3351–3356. <https://doi.org/10.1021/ac050080v>
30. Dobbelin M, Ciesielski A, Haar S, Haar S, Osella S, Bruna M, Minoia A, De Cola L (2016) Light-enhanced liquid-phase exfoliation and current photoswitching in graphene-azobenzene composites. *Nat Commun* 7:11090. <https://doi.org/10.1038/ncomms11090>
31. Haar S, El Gemayel M, Shin Y, Melinte G, Squillaci MA, Ersen O, Samori P (2015) Enhancing the liquid-phase exfoliation of graphene in organic solvents upon addition of noctylbenzene. *Sci Rep* 5(1):16684. <https://doi.org/10.1038/srep16684>
32. Li F, Shi JJ, Qin X (2010) Synthesis and supercapacitor characteristics of PANI/CNTs composites. *Chinese sci bull* 55(11):1100–1106. <https://doi.org/10.1007/s11434-009-0573-9>
33. Hu L, Tu J, Jiao S, Hou J, Zhu H, Fray DJ (2012) In situ electrochemical polymerization of a nanorod-PANI-graphene composite in a reverse micelle electrolyte and its application in a supercapacitor. *Phys Chem Chem Phys* 14(45):15652–15656. <https://doi.org/10.1039/c2cp42192e>
34. Du X, Wang C, Chen M, Jiao Y, Wang J (2016) Electrochemical performances of nanoparticle Fe_3O_4 /activated carbon supercapacitor using KOH electrolyte solution. *J Phys Chem C* 113:2643–2646
35. Li L, Dou Y, Wang L, Luo M, Liang J (2014) One-step synthesis of high-quality N-doped graphene/ Fe_3O_4 hybrid nanocomposite and its improved supercapacitor performances. *RSC Adv* 4(49):25658–25665. <https://doi.org/10.1039/C4RA02962C>
36. Oh I, Kim M, Kim J (2015) Fe_3O_4 /carbon coated silicon ternary hybrid composite as supercapacitor electrodes. *Appl Surf Sci* 328:222–228. <https://doi.org/10.1016/j.apsusc.2014.12.066>
37. Liao Q, Li N, Jin S, Yang G, Wang C (2015) All-solid-state symmetric supercapacitor based on Co_3O_4 nanoparticles on vertically aligned graphene. *ACS Nano* 9(5):5310–5317. <https://doi.org/10.1021/acsnano.5b00821>
38. Liu W, Li X, Zhu M, He X (2015) High-performance all-solid state asymmetric supercapacitor based on Co_3O_4 nanowires and carbon aerogel. *J Power Sources* 282:179–186. <https://doi.org/10.1016/j.jpowsour.2015.02.047>
39. Wang L, Ji H, Wang S, Kong L, Jiang X, Yang G (2013) Preparation of Fe_3O_4 with high specific surface area and improved capacitance as a supercapacitor. *Nano* 5:3793–3799
40. Wang L, Yu J, Dong X, Li X, Xie Y, Chen S, Li P, Hou H, Song Y (2016) Three-dimensional macroporous carbon/ Fe_3O_4 -doped porous carbon nanorods for high-performance supercapacitor. *ACS Sustain Chem Eng* 4(3):1531–1537. <https://doi.org/10.1021/acssuschemeng.5b01474>
41. Wang L, Zhang Y, Li X, Xie Y, He J, Yu J, Song Y (2015) The MIL-88A-derived Fe_3O_4 -carbon hierarchical nanocomposites for electrochemical sensing. *Sci Rep* 5(1):14341. <https://doi.org/10.1038/srep14341>
42. Song Y, JL X, Liu XX (2014) Electrochemical anchoring of dual doping polypyrrole on graphene sheets partially exfoliated from graphite foil for high-performance supercapacitor electrode. *J Power Sources* 249:48–58. <https://doi.org/10.1016/j.jpowsour.2013.10.102>
43. Lang L, Xu Z (2013) In situ synthesis of porous $\text{Fe}_3\text{O}_4/\text{C}$ microbelts and their enhanced electrochemical performance for lithium-ion batteries. *ACS Applied Mater Inter* 5(5):1698–1703. <https://doi.org/10.1021/am302753p>
44. Pardieu E, Pronkin SN, Dolci M, Dintzer T, Pichon BP, Begin D, Boulmedais F (2015) Hybrid layer-by-layer composites based on conducting polyelectrolyte and Fe_3O_4 nanostructures grafted on graphene for supercapacitors application. *J Mater Chem A* 3(45):22877–22885. <https://doi.org/10.1039/C5TA05132K>
45. Yan F, Ding J, Liu Y, Wang Z, Cai Q, Zhang J (2015) Fabrication of magnetic irregular hexagonal- Fe_3O_4 sheets/reduced graphene oxide composite for supercapacitors. *Synthetic Met* 209:473–479. <https://doi.org/10.1016/j.synthmet.2015.08.023>
46. Li F, Chen H, Liu XY, Zhu SJ, Jia JQ, CH X, Zhang YX (2015) Low-cost high-performance asymmetric supercapacitors based on $\text{Co}_2\text{AlO}_4/\text{MnO}_2$ nanosheets and Fe_3O_4 nanoflakes. *J Mater Chem A* 4:2096–2104
47. Zeng X, Yang B, Li X, Li R, Yu R (2016) Solvothermal synthesis of hollow Fe_3O_4 sub-micron spheres and their enhanced electrochemical properties for supercapacitors. *Mater Design* 101:35–43. <https://doi.org/10.1016/j.matdes.2016.03.155>
48. Liu J, Liu S, Zhuang S, Wang X, Tu F (2013) Synthesis of carbon-coated Fe_3O_4 nanorods as electrode material for supercapacitor. *Ionics* 19(9):1255–1261. <https://doi.org/10.1007/s11581-013-0857-6>
49. Mu J, Chen B, Guo Z, Zhang M, Zhang Z, Zhang P, Shao C, Liu Y (2011) Highly dispersed Fe_3O_4 nanosheets on one-dimensional carbon nanofibers: synthesis, formation mechanism, and electrochemical performance as supercapacitor electrode materials. *Nano* 3:5034–5040
50. Shi W, Zhu J, Sim D, Tay Y, Lu Z, Zhang X, Sharma Y, Srinivasan M, Zhang H (2011) Achieving high specific charge capacitances in Fe_3O_4 /reduced graphene oxide nanocomposites. *J Mater Chem* 21(10):3422–3427. <https://doi.org/10.1039/c0jm03175e>
51. Khoh W, Hong J (2013) Layer-by-layer self-assembly of ultrathin multilayer films composed of magnetite/reduced graphene oxide bilayers for supercapacitor application. *Colloids Surf A Physicochem Eng Asp* 436:104–112. <https://doi.org/10.1016/j.colsurfa.2013.06.012>